Uniformly stable wavelets on nonuniform triangulations

Solveig Bruvoll[a,c], Tom Lyche[b], Knut Mørken[b]

[a] *Department of informatics, University of Oslo, Norway*
[b] *Department of mathematics, University of Oslo, Norway*
[c] *Norwegian Defence Research Establishment (FFI), P.O. Box 25, NO-2027 Kjeller, Norway (Present address)*

Abstract

In this paper we construct linear, uniformly stable, wavelet-like functions on arbitrary triangulations. As opposed to standard wavelets, only local orthogonality is required for the wavelet-like functions. Nested triangulations are obtained through refinement by two standard strategies, in which no regularity is required. One strategy inserts a new node at an arbitrary position inside a triangle and then splits the triangle into three smaller triangles. The other strategy splits two neighboring triangles into four smaller triangles by inserting a new node somewhere on the edge between the triangles. In other words, non-uniform refinement is allowed in both strategies. The refinement results in nested spaces of piecewise linear functions. The detail-, or wavelet-spaces, are made to satisfy certain orthogonality conditions which locally correspond to vanishing linear moments. It turns out that this construction is uniformly stable in the L_∞ norm, independently of the geometry of the original triangulation and the refinements.

Keywords: wavelets, approximation, stability, non-uniform triangulations

1. Introduction

Wavelets have become a popular tool in many areas of mathematics and science. Classical wavelets were defined on regular uniform grids over the whole

*Corresponding author
Email address: `solveig.bruvoll@ffi.no` (Solveig Bruvoll)

DOI til publisert versjon / DOI to published version: 10.1016/j.matcom.2016.09.006

real line and were required to satisfy strong orthogonality conditions [4]. Early extensions relaxed the orthogonality conditions and provided simple restrictions to intervals, cf, [2]. The use of spline wavelets provided better treatment of boundary conditions on intervals, as well as a natural construction of wavelets on non-uniform grids, as shown in [1], [3] and [8].

Any univariate construction, including wavelets, can be extended to the multivariate setting by the standard tensor product construction. Various kinds of wavelets have also been constructed on triangulations, but to our knowledge, the most general setting for these constructions is a non-uniform base triangulation with some kind of uniform refinement rule, see e.g. [5], [6], [7], [10], and [11].

Construction of wavelets over irregular grids raises an additional issue, namely whether the construction is stable independently of the grid geometry. It was recently shown in [9] that this is indeed the case for univariate, linear wavelets on irregular grids with vanishing moments when the stability is measured in the uniform norm.

The purpose of the present paper is to generalize the results in [9] to linear wavelets over general triangulations. Linear wavelets that are locally orthogonal to the original basis of hat functions are constructed. We use two standard, but not widely used, refinement rules, which both allow non-uniform refinement. These wavelets are shown to be uniformly stable, independently of the topology and geometry of both the original triangulation and the refinements. As in [9] we measure stability in the uniform norm. We limit our studies to general triangulations that can be projected onto a plane.

In section 2 we give a brief overview of the construction. In section 3 we discuss the first refinement strategy in detail, including stability results, and in section 4 we discuss the second strategy. In section 5 we then combine these results and consider iterated refinement with a combination of the two strategies. We end with some examples in section 6 and conclude in section 7.

DOI til publisert versjon / DOI to published version: 10.1016/j.matcom.2016.09.006

2. An overview of the wavelet construction

Let N be a finite set of points in $\mathbb{R}^2$, usually referred to as nodes. Any set of three nodes forms a triangle, and a triangulation Δ over N is a collection of triangles with the property that two triangles in Δ are either disjunct, or have a vertex or edge in common. We will refer to the number of edges emanating from a node as its valence. For each node $\boldsymbol{v} \in N$ we construct the linear B-spline (hat function) $\phi_{\boldsymbol{v}}$ with the property that for any two nodes $\alpha, \beta \in N$ we have $\phi_\alpha(\beta) = \delta_{\alpha\beta}$.

We start with an arbitrary base triangulation Δ_0 defined over an initial set N_0 of nodes. We then refine the base triangulation through node insertions, where each node is inserted according to one of two alternative strategies. The first strategy is to insert a new node $\boldsymbol{p}$ in the interior of a triangle $T = (\boldsymbol{v}_0, \boldsymbol{v}_1, \boldsymbol{v}_2)$ and split the triangle into three smaller triangles, as shown in figure 1(a). The inserted point $\boldsymbol{p}$ can then be expressed as a convex combination of $\boldsymbol{v}_0, \boldsymbol{v}_1$ and $\boldsymbol{v}_2$ by $\boldsymbol{p} = a_0\boldsymbol{v}_0 + a_1\boldsymbol{v}_1 + a_2\boldsymbol{v}_2$, where $\boldsymbol{a} = (a_0, a_1, a_2)$ contains the barycentric coordinates of the point $\boldsymbol{p}$, i.e., they satisfy $a_i \geq 0$ and $\sum_{i=0}^{2} a_i = 1$. For $\boldsymbol{p}$ to be inserted inside the triangle, we require $0 < a_i < 1$. The second strategy for node insertion is to insert the new node $\boldsymbol{p}$ along an edge $e = (\boldsymbol{v}_0, \boldsymbol{v}_1)$ and divide each of the two triangles sharing the edge into two new triangles, as shown in figure 1(b). The new node can now be expressed as $\boldsymbol{p} = \lambda\boldsymbol{v}_0 + (1-\lambda)\boldsymbol{v}_1$, where $0 < \lambda < 1$. Regardless of the insertion strategy, we can construct a new hat function $\sigma_{\boldsymbol{p}}$, such that $\sigma_{\boldsymbol{p}}(\boldsymbol{p}) = 1$ and $\sigma_{\boldsymbol{p}}(\boldsymbol{v}) = 0$ for all nodes $\boldsymbol{v} \in N_0$. In either case we denote the new set of nodes $N_0 \cup \{\boldsymbol{p}\}$ by N_1 and the new triangulation by Δ_1.

If we allow one or more $a_i \in \{0, 1\}$ or $\lambda \in \{0, 1\}$ for an inserted knot $\boldsymbol{p}$, the corresponding hat function $\sigma_{\boldsymbol{p}}$ will be discontinuous. For simplicity we will not discuss these cases in this paper.

We will now give an overview of our wavelet construction for node insertion strategy 1. Strategy 2 is treated later in a similar way. The set $\boldsymbol{\phi} = \{\phi_{\boldsymbol{v}} \mid \boldsymbol{v} \in N_0\}$ forms a basis for the space $\mathbb{V}_0 = \mathbb{V}(\Delta_0)$ of continuous functions that

DOI til publisert versjon / DOI to published version: 10.1016/j.matcom.2016.09.006

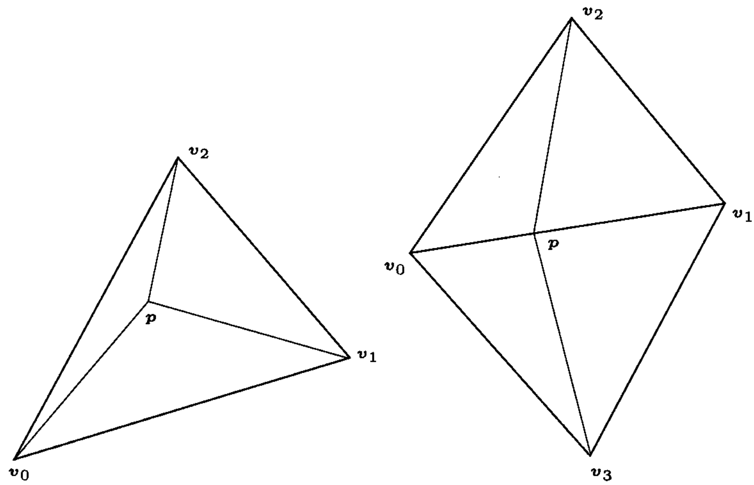

(a) Insertion of a node inside a triangle. (b) Node insertion on an edge.

Figure 1: The two strategies for refining a triangulation.

are linear on each triangle in Δ_0. Similarly, the set $\boldsymbol{\gamma} = \{\gamma_v \mid v \in N_1\}$ forms a basis for the refined space $\mathbb{V}_1$, and it is well-known that $\mathbb{V}_0 \subseteq \mathbb{V}_1$. The natural generalisation of the construction in [9] is to construct an alternative basis $\{\boldsymbol{\phi}, \hat{\psi}_{\boldsymbol{p}}\}$ for $\mathbb{V}_1$ with the property that

$$\int_{\mathbb{R}^2} \hat{\psi}_{\boldsymbol{p}} g = 0, \quad \text{for } g = 1, x, y,$$

Here $\hat{\psi}_{\boldsymbol{p}} = \gamma_{\boldsymbol{p}} - \sum_{i=0}^{2} c_i \phi_{\boldsymbol{v}_i}$, where $\boldsymbol{v}_i$ are the vertices of the triangle that contains $\boldsymbol{p}$, and $(c_i)_{i=0}^{2}$ are certain coefficients $(c_i)_{i=0}^{2}$ to be determined. These equations constitute a linear system of equations for determining the unknown coefficients, but unfortunately, it turns out that this construction is not stable independently of the geometry. More specifically, there exist triangulations such that the resulting linear system of equations is singular. An example of such a triangulation is shown in figure 2.

We want to construct an alternative basis $\{\boldsymbol{\phi}, \psi_{\boldsymbol{p}}\}$ for $\mathbb{V}_1$ with the property that the function $\psi_{\boldsymbol{p}}$ satisfies the orthogonality condition

$$\int \phi_{\boldsymbol{v}} \psi_{\boldsymbol{p}} = 0 \tag{1}$$

DOI til publisert versjon / DOI to published version: 10.1016/j.matcom.2016.09.006

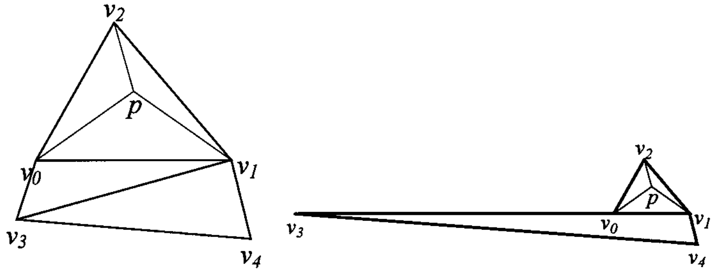

Figure 2: An example of a triangulation that causes problems if we require vanishing moments with 1, x, and y when inserting the node $\boldsymbol{p}$. The left figure shows the topology of the triangulation, while the right figure shows a position of the node $\boldsymbol{v}_3$ for which the associated linear system of equations is singular. Note that the topology in both triangulations is the same. In the right triangulation, some of the triangles are deformed, but they have not collapsed.

for all $\boldsymbol{v} \in N$ for which $\phi_{\boldsymbol{v}}$ is not identically equal to zero on the support of $\sigma_{\boldsymbol{p}}$, i.e., for all $\boldsymbol{v}$ in the ring around $\boldsymbol{p}$. For strategy I there will be three such hat functions, based at the three vertices surrounding $\boldsymbol{p}$ in figure 1(a). For strategy II we see from figure 1(b) that there will be four such functions. We construct $\psi_{\boldsymbol{p}}$ by finding constants c_i such that the function

$$\psi_{\boldsymbol{p}} = \gamma_{\boldsymbol{p}} - \sum_{i=0}^{n-1} c_i \phi_{\boldsymbol{v}_i} \tag{2}$$

satisfies the orthogonality conditions, with $n = 3$ for the first strategy and $n = 4$ for the second. This is a standard way to adjust wavelets, see e.g. [12].

In practice, the sets of nodes N_0 and N_1, as well as the basis functions ϕ and γ, will necessarily be listed in some order. However, the particular ordering employed is not essential.

3. Node insertion according to strategy I

3.1. Defining equations

A triangle $T_0 = (\boldsymbol{v}_0, \boldsymbol{v}_1, \boldsymbol{v}_2)$ is refined by inserting a node $\boldsymbol{p}$ as shown in figure 1(a). We want to construct the corresponding wavelet function $\psi_{\boldsymbol{p}}$ given

DOI til publisert versjon / DOI to published version: 10.1016/j.matcom.2016.09.006

by (2) such that it satisfies the three conditions (1) with $\boldsymbol{v} = \boldsymbol{v}_i$ for $i = 0$, 1, 2. In other words

$$\psi_{\boldsymbol{p}} = \gamma_{\boldsymbol{p}} - c_0\phi_{\boldsymbol{v}_0} - c_1\phi_{\boldsymbol{v}_1} - c_2\phi_{\boldsymbol{v}_2}, \tag{3}$$

and we determine the three coefficients c_0, c_1 and c_2 by solving the linear system

$$\begin{bmatrix} \int \phi_{\boldsymbol{v}_0}\phi_{\boldsymbol{v}_0} & \int \phi_{\boldsymbol{v}_0}\phi_{\boldsymbol{v}_1} & \int \phi_{\boldsymbol{v}_0}\phi_{\boldsymbol{v}_2} \\ \int \phi_{\boldsymbol{v}_1}\phi_{\boldsymbol{v}_0} & \int \phi_{\boldsymbol{v}_1}\phi_{\boldsymbol{v}_1} & \int \phi_{\boldsymbol{v}_1}\phi_{\boldsymbol{v}_2} \\ \int \phi_{\boldsymbol{v}_2}\phi_{\boldsymbol{v}_0} & \int \phi_{\boldsymbol{v}_2}\phi_{\boldsymbol{v}_1} & \int \phi_{\boldsymbol{v}_2}\phi_{\boldsymbol{v}_2} \end{bmatrix} \begin{bmatrix} c_0 \\ c_1 \\ c_2 \end{bmatrix} = \begin{bmatrix} \int \phi_{\boldsymbol{v}_0}\gamma_{\boldsymbol{p}} \\ \int \phi_{\boldsymbol{v}_1}\gamma_{\boldsymbol{p}} \\ \int \phi_{\boldsymbol{v}_2}\gamma_{\boldsymbol{p}} \end{bmatrix}.$$

For reference, we let this linear system be denoted by

$$\boldsymbol{M}_I \boldsymbol{x}_I = \boldsymbol{F}_I. \tag{4}$$

The integrals in $\boldsymbol{M}_I$ can be expressed explicitly, since the functions $\phi_{\boldsymbol{v}}$ and $\gamma_{\boldsymbol{p}}$ are linear B-splines. As shown in [6], the integral $\int_T fg$ for two linear functions f and g over a triangle $T = \{\boldsymbol{v}_0, \boldsymbol{v}_1, \boldsymbol{v}_2\}$ can be expressed as

$$\int_T fg = \frac{A(T)}{12} h_T(f, g), \tag{5}$$

where $A(T)$ is the area of T and

$$h_T(f, g) = f_0 g_0 + f_1 g_1 + f_2 g_2 + (f_0 + f_1 + f_2)(g_0 + g_1 + g_2). \tag{6}$$

The values f_i and g_i for $i = 0, 1, 2$ are the values of the functions f and g evaluated at the vertex $\boldsymbol{v}_i$ of T.

Let S_α denote the support of ϕ_α and $S_{\alpha\beta} = S_\alpha \cap S_\beta$ for nodes $\alpha, \beta \in N$. Also let $A(S_\alpha)$ denote the area of S_α. Then the integrals can be expressed by

$$\int \phi_\alpha \phi_\beta = \begin{cases} A(S_\alpha)/6, & \alpha = \beta; \\ A(S_{\alpha\beta})/12, & \alpha \neq \beta; \end{cases} \tag{7}$$

and

$$\int \phi_{\boldsymbol{v}_i} \gamma_{\boldsymbol{p}} = \frac{1}{12} A(S_{\boldsymbol{p}})(a_i + 1), \tag{8}$$

where a_i is the barycentric coordinate of $\boldsymbol{v}_i$ in the expression for node $\boldsymbol{p}$,

$$\boldsymbol{p} = a_0 \boldsymbol{v}_0 + a_1 \boldsymbol{v}_1 + a_2 \boldsymbol{v}_2, \tag{9}$$

DOI til publisert versjon / DOI to published version: 10.1016/j.matcom.2016.09.006

and S_p is the support of γ_p.

We now divide the total support of the hat functions in the system as shown in figure 3. For $i = 0, 1, 2, 3$, T_i denotes a triangle, while for $i = 4, 5, 6$, T_i denotes a set of triangles. More explicitly, T_4 denotes all triangles with a common vertex at $\boldsymbol{v}_0$, except for the three explicitly indicated triangles T_0, T_1 and T_3, and similarly for T_5 and T_6. For $i = 0 \ldots 6$, the area of T_i is denoted by $A_i = A(T_i)$. From the formulas (7) and (8) we then see that the matrix $\boldsymbol{M}_I$ and the vector $\boldsymbol{F}_I$ can be expressed by

$$\boldsymbol{M}_I = \tfrac{1}{12} \begin{bmatrix} 2(A_0 + A_1 + A_3 + A_4) & A_0 + A_1 & A_0 + A_3 \\ A_0 + A_1 & 2(A_0 + A_1 + A_2 + A_5) & A_0 + A_2 \\ A_0 + A_3 & A_0 + A_2 & 2(A_0 + A_2 + A_3 + A_6) \end{bmatrix} \tag{10}$$

and

$$\boldsymbol{F}_I = \frac{A_0}{12} \begin{bmatrix} a_0 + 1 \\ a_1 + 1 \\ a_2 + 1 \end{bmatrix}. \tag{11}$$

These are the basic equations that govern the construction of the wavelet functions.

3.2. Bounding the coefficients

When only one new node is inserted, the challenge in constructing wavelets that are uniformly stable is to bound the coefficients $\boldsymbol{x} = (c_0, c_1, c_2)$ independently of the triangulation and its refinement. We first record some properties of the matrix $\boldsymbol{M}_I$.

Lemma 1. *The determinant of $\boldsymbol{M}_I$ is nonnegative, and* $\det \boldsymbol{M}_I > 0$ *if the triangle T_0 that is refined has nonzero area. Let $\boldsymbol{M}_i$ denote the submatrix of $\boldsymbol{M}_I$ obtained by removing column 1 and row i, and set $D_i = \det \boldsymbol{M}_i$. Then $D_1 > |D_2|$ and $D_1 > |D_3|$.*

Proof. The B-splines ϕ_i are linearly independent provided that the triangle T_0 that is being refined has nonzero area, and it is well-known that a Gram

DOI til publisert versjon / DOI to published version: 10.1016/j.matcom.2016.09.006

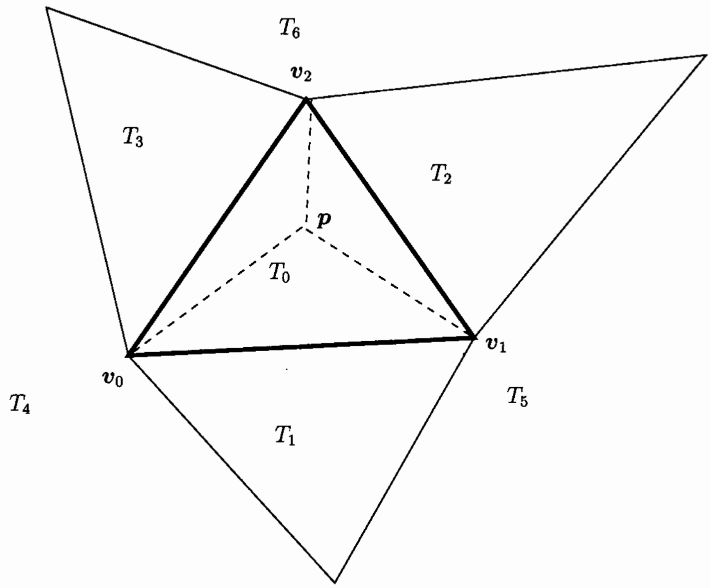

Figure 3: Overview of the regions involved in the equations for strategy I. Note that T_4 denotes the region defined by all the triangles with a common vertex at v_0, except for the three explicitly indicated triangles T_0, T_1 and T_3. The same applies to T_5 and T_6. The area of region T_k is denoted by A_k.

DOI til publisert versjon / DOI to published version: 10.1016/j.matcom.2016.09.006

matrix of linearly independent functions has a positive determinant. To derive the relations between the sub-determinants one may for example check that all four inequalities

$$D_1 - D_2 > 0, \quad D_1 - D_3 > 0,$$

$$D_1 + D_2 > 0, \quad D_1 + D_3 > 0$$

hold — this follows quite easily by simply expanding the determinants.

To bound the coefficients, we partition the matrix $\boldsymbol{M}_I$ by its columns as $\boldsymbol{M}_I = [\boldsymbol{m}_1, \boldsymbol{m}_2, \boldsymbol{m}_3]$ (note that we include the factor $1/12$ in each of the columns). By Cramer's rule, the solution of (4) is then given by

$$c_0 = \frac{\det[\boldsymbol{F}, \boldsymbol{m}_2, \boldsymbol{m}_3]}{\det \boldsymbol{M}_I}, \quad c_1 = \frac{\det[\boldsymbol{m}_1, \boldsymbol{F}, \boldsymbol{m}_3]}{\det \boldsymbol{M}_I}, \quad c_2 = \frac{\det[\boldsymbol{m}_1, \boldsymbol{m}_2, \boldsymbol{F}]}{\det \boldsymbol{M}_I}. \tag{12}$$

Because of symmetry, it is sufficient to obtain a bound for one of the coefficients, say c_0.

Lemma 2. *The coefficient c_0 is bounded by*

$$|c_0| \leq \frac{A_0}{A_0 + A_4 + 6(A_1 + A_3)/7} \tag{13}$$

where the A_is denote the areas of the corresponding triangles in figure 3.

Proof. The coefficient c_0 is given by

$$c_0 = \frac{\det[\boldsymbol{F}_I, \boldsymbol{m}_2, \boldsymbol{m}_3]}{\det \boldsymbol{M}_I},$$

and we know that $\det \boldsymbol{M}_I > 0$. We observe that by (8),

$$\det[\boldsymbol{F}_I, \boldsymbol{m}_2, \boldsymbol{m}_3] = \frac{A_0}{12}\big(\det[\mathbf{1}, \boldsymbol{m}_2, \boldsymbol{m}_3] + \det[\boldsymbol{a}, \boldsymbol{m}_2, \boldsymbol{m}_3]\big),$$

where $\mathbf{1} = (1,1,1)^T$ and $\boldsymbol{a} = (a_0, a_1, a_2)^T$ are the barycentric coordinates of $\boldsymbol{p}$. We claim that when $\boldsymbol{a}$ varies, the right-hand side reaches its maximum when $\boldsymbol{a} = (1,0,0)^T$. To see this, we note that

$$\det[\boldsymbol{a}, \boldsymbol{m}_2, \boldsymbol{m}_3] = a_0 D_1 + a_1(-D_2) + a_2 D_3.$$

In other words $\det[\boldsymbol{a}, \boldsymbol{m}_2, \boldsymbol{m}_3]$ is a convex combination of the three numbers D_1, $-D_2$, D_3, and is therefore bounded by the one that is largest in absolute

DOI til publisert versjon / DOI to published version: 10.1016/j.matcom.2016.09.006

value. From lemma 1 we know that this is D_1 which corresponds to $a_0 = 1$ and $a_1 = a_2 = 0$. It is also easy to see that $\det[\boldsymbol{F}_I, \boldsymbol{m}_2, \boldsymbol{m}_3]$ is positive for this value of $\boldsymbol{a}$. Then

$$c_0 \leq \frac{A_0}{12} \frac{\det[\boldsymbol{v}, \boldsymbol{m}_2, \boldsymbol{m}_3]}{\det \boldsymbol{M}_I},$$

where $\boldsymbol{v} = [2, 1, 1]^T$. To derive our final upper bound, we want to show that

$$\frac{A_0 \det[\boldsymbol{v}, \boldsymbol{m}_2, \boldsymbol{m}_3]}{12 \det \boldsymbol{M}_I} \leq \frac{A_0}{B}, \tag{14}$$

where B is some linear combination of the areas A_0, A_1, A_3, and A_4.

If we expand the determinants by the first column and make use of the subdeterminants, the inequality (14) can be written

$$(2D_1 - D_2 + D_3)B \leq 2(A_0 + A_1 + A_3 + A_4)D_1 - (A_0 + A_1)D_2 + (A_0 + A_3)D_3.$$

We introduce a new variable B_1 via the relation $B = A_0 + B_1$. This allows us to eliminate A_0 from the inequality,

$$(2D_1 - D_2 + D_3)B_1 \leq 2(A_1 + A_3 + A_4)D_1 - A_1 D_2 + A_3 D_3.$$

Because of the symmetry between A_1 and A_3 in the construction, we must have $B_1 = b_1(A_1 + A_3) + b_2 A_4$ fore some constants b_1 and b_2. From the last inequality it is reasonable to choose $b_2 = 1$. Some trial and error with Mathematica indicates that $b_1 = 6/7$ is a good choice, and one can check (most easily with a tool like Mathematica) that the inequality holds for these values of the b_is. In other words, inequality (14) holds when $B = A_0 + A_4 + 6(A_1 + A_3)/7$, as we wanted to show. These values for b_1 and b_2 ensure positivity, but are not optimal. Therefore the upper bound in equation 13 is not in general the smallest upper bound.

3.3. Insertion of several nodes

One may consider insertion of many nodes according to strategy I as repeated insertions of one node, or as fewer repeated insertions, but with more than one node each time. When analysing stability, it turns out that it is advantageous

DOI til publisert versjon / DOI to published version: 10.1016/j.matcom.2016.09.006

to use the latter point of view and for example consider one step as insertion of one node in each triangle.

Recall that the functions $\boldsymbol{\phi} = \{\phi_{\boldsymbol{v}} \mid \boldsymbol{v} \in N_0\}$ form a basis for the set $\mathbb{V}_0$ of linear functions over the base triangulation Δ_0. After insertion of several nodes according to strategy 1, but at most one in each triangle, we denote the new set of nodes by N_1 and the new triangulation by Δ_1. A natural basis for the set $\mathbb{V}_1$ of linear functions over Δ_1, is the set $\boldsymbol{\gamma} = \{\gamma_\alpha \mid \alpha \in N_1\}$ consisting of all the linear B-splines in $\mathbb{V}_1$. A general function f_1 in $\mathbb{V}_1$ is then given by

$$f_1 = \boldsymbol{\gamma}^T \boldsymbol{b} = \sum_{\alpha \in N_1} \gamma_\alpha b_\alpha, \tag{15}$$

where $\boldsymbol{b} = (\boldsymbol{b}_\alpha)$ is a suitable coefficient vector. Since the B-splines satisfy $\gamma_\alpha(\beta) = \delta_{\alpha\beta}$ for any $\alpha, \beta \in N_1$, we have $f_1(\boldsymbol{v}_i) = \boldsymbol{b}_{\boldsymbol{v}_i}$.

It is not difficult to see that an alternative basis for $\mathbb{V}_1$ is given by the set $\{\boldsymbol{\phi}, \boldsymbol{\psi}\}$, where $\boldsymbol{\psi} = \{\psi_{\boldsymbol{v}} \mid \boldsymbol{v} \in N_1 \backslash N_0\}$. This means that there are coefficients $\boldsymbol{d}$ and $\boldsymbol{w}$ such that

$$f_1 = \boldsymbol{\gamma}^T \boldsymbol{b} = \boldsymbol{\phi}^T \boldsymbol{d} + \boldsymbol{\psi}^T \boldsymbol{w} = f_0 + g_0. \tag{16}$$

The forward wavelet transform amounts to changing the representation of f_1 from the basis $\boldsymbol{\gamma}$ to the basis $(\boldsymbol{\phi}, \boldsymbol{\psi})$, while the inverse wavelet transform corresponds to the inverse change of basis.

We will now examine the wavelet transforms in some more detail by establishing the relation between the coefficients $\boldsymbol{w}$, $\boldsymbol{d}$ and $\boldsymbol{b}$. We first find a matrix relation between the basis functions $\boldsymbol{\psi}$, $\boldsymbol{\phi}$ and $\boldsymbol{\gamma}$ and then use this to obtain more direct relations between the coefficients.

It is useful to reorder the basis functions in $\boldsymbol{\gamma}$ as $\{\gamma_O, \gamma_N\}$, where

$$\gamma_O = \{\gamma_{\boldsymbol{v}} \mid \gamma_{\boldsymbol{v}}(\boldsymbol{v}) = 1 \text{ for } \boldsymbol{v} \in N_0\},$$

the set of fine hat functions that are equal to one at an old node, and

$$\gamma_N = \{\gamma_{\boldsymbol{v}} \mid \gamma_{\boldsymbol{v}}(\boldsymbol{v}) = 1 \text{ for } \boldsymbol{v} \in N_1 \backslash N_0\},$$

those that are equal to one at a new (inserted) node. We will establish the

DOI til publisert versjon / DOI to published version: 10.1016/j.matcom.2016.09.006

relation between the two bases $\{\boldsymbol{\phi}, \boldsymbol{\psi}\}$ and $\boldsymbol{\gamma}$ by a two-step conversion via the basis $\{\boldsymbol{\phi}, \boldsymbol{\gamma}_N\}$, as done in [9].

We start by finding the relation between the two bases $\{\boldsymbol{\phi}, \boldsymbol{\psi}\}$ and $\{\boldsymbol{\phi}, \boldsymbol{\gamma}_N\}$. From equation (3), we know that for each node $\boldsymbol{v}_r \in N_1 \backslash N_0$ inserted in a triangle $T_r = (\boldsymbol{v}_i, \boldsymbol{v}_j, \boldsymbol{v}_k)$, the function $\psi_{\boldsymbol{v}_r}$ is given by

$$\psi_{\boldsymbol{v}_r} = \gamma_{\boldsymbol{v}_r} - c_i^r \phi_{\boldsymbol{v}_i} - c_j^r \phi_{\boldsymbol{v}_j} - c_k^r \phi_{\boldsymbol{v}_k}, \tag{17}$$

where the coefficients c_i^r, c_j^r, c_k^r are found by solving the linear system (4) corresponding to insertion of node $\boldsymbol{v}_r$. We construct a matrix $\boldsymbol{C}$, where each element in column r is zero, except for the three entries c_i^r, c_j^r, c_k^r in the positions corresponding to the basis functions ϕ_{v_i}, ϕ_{v_j}, and ϕ_{v_r}. Row i of $\boldsymbol{C}$ contains every nonzero c_i^r used as a coefficient for $\phi_{\boldsymbol{v}_i}, \boldsymbol{v}_i \in N_0$ in any expression for a $\psi_{\boldsymbol{v}_r}, \boldsymbol{v}_r \in N_1 \backslash N_0$. The number of nonzero entries in row i is equal to the number of neighboring triangles $T \in \Delta_0$ to node $\boldsymbol{v}_i$ in which a new node $\boldsymbol{v}_r$ is inserted. This allows us to express the relation between the two bases $\{\boldsymbol{\phi}, \boldsymbol{\psi}\}$ and $\{\boldsymbol{\phi}, \boldsymbol{\gamma}_N\}$ by

$$\left[\ \boldsymbol{\phi}^T, \boldsymbol{\psi}^T\ \right] = \left[\ \boldsymbol{\phi}^T, \boldsymbol{\gamma}_N^T\ \right] \begin{bmatrix} \boldsymbol{I} & -\boldsymbol{C} \\ 0 & \boldsymbol{I} \end{bmatrix} = \left[\ \boldsymbol{\phi}^T, -\boldsymbol{\phi}^T \boldsymbol{C} + \boldsymbol{\gamma}_N^T\ \right].$$

We now turn to the relation between the two bases $\{\boldsymbol{\phi}, \boldsymbol{\gamma}_N\}$ and $\boldsymbol{\gamma}$. We know that the basis functions in $\boldsymbol{\gamma}_N$ are just a subset of the total basis $\boldsymbol{\gamma}$ for $\mathbb{V}_1$. The main challenge is therefore to express the coarse hat functions $\boldsymbol{\phi}$ in terms of the fine hat functions $\boldsymbol{\gamma}$ — this is possible since $\mathbb{V}_0 \subseteq \mathbb{V}_1$. Let us consider one such basis function $\phi_{\boldsymbol{v}_i}$ for some $\boldsymbol{v}_i \in N_0$. This function can be expressed by a linear combination of $\gamma_{\boldsymbol{v}_i}$ and the hat functions $\gamma_{\boldsymbol{v}_r}$ for $\boldsymbol{v}_r \in N_1 \backslash N_0$, for which there exists a triangle $T \in \Delta_1$ such that $\boldsymbol{v}_i, \boldsymbol{v}_r \in T$. Let L_i be the set of indices corresponding to these hat functions $\gamma_{\boldsymbol{v}_r}$. We recall that when a node $\boldsymbol{v}_r$ is inserted in a triangle $T_r = (\boldsymbol{v}_i, \boldsymbol{v}_j, \boldsymbol{v}_k) \in \Delta_0$, it can be expressed as the weighted sum $\boldsymbol{v}_r = a_i^r \boldsymbol{v}_i + a_j^r \boldsymbol{v}_j + a_k^r \boldsymbol{v}_k$, where the weights are the barycentric coordinates of $\boldsymbol{v}_r$. Then it is well-known that

$$\phi_{\boldsymbol{v}_i} = \gamma_{\boldsymbol{v}_i} + \sum_{r \in L_i} a_i^r \gamma_{\boldsymbol{v}_r}, \tag{18}$$

DOI til publisert versjon / DOI to published version: 10.1016/j.matcom.2016.09.006

where a_i^r is the barycentric coordinate of vertex $\boldsymbol{v}_i$ in the expression for $\boldsymbol{v}_r$ over T_r.

Equation 18 may be expressed in matrix form by introducing a matrix $\boldsymbol{A}$ consisting of zeros and the barycentric coordinates a_i^r of the inserted nodes $\boldsymbol{v}_r \in N_1 \backslash N_0$. At the appropriate positions in row r of $\boldsymbol{A}$, we have the three barycentric coordinates a_i^r of the new knot $\boldsymbol{v}_r$ inserted in triangle T_r. These three entries are the only non-zero entries in row r, and they will always sum to one. In each column i, we have one entry for each element of the set L_i, and entry r is the barycentric coordinate a_i^r of the original knot $\boldsymbol{v}_i \in N_0$ in the expression for the new knot $\boldsymbol{v}_r \in N_1 \backslash N_0$.

The matrix $\boldsymbol{A}$ allows us to write equation 18 in matrix form. If we augment this relation with the new hat functions γ_N, we obtain the desired relation between the two bases $\{\boldsymbol{\phi}, \gamma_N\}$ and γ,

$$\left[\ \boldsymbol{\phi}^T, \gamma_N^T\ \right] = \left[\ \gamma_O^T, \gamma_N^T\ \right] \begin{bmatrix} \boldsymbol{I} & 0 \\ \boldsymbol{A} & \boldsymbol{I} \end{bmatrix} = \left[\ \gamma_O^T + \gamma_N^T \boldsymbol{A}, \gamma_N^T\ \right]. \tag{19}$$

This in turn leads to the desired relation between the two bases $\{\boldsymbol{\phi}, \boldsymbol{\psi}\}$ and γ.

Lemma 3. *The space $\mathbb{V}_1$ has the two bases $\{\boldsymbol{\phi}, \boldsymbol{\psi}\}$ and γ which are related by*

$$\left[\boldsymbol{\phi}^T, \boldsymbol{\psi}^T\right] = \left[\gamma_O^T, \gamma_N^T\right] \begin{bmatrix} \boldsymbol{I} & 0 \\ \boldsymbol{A} & \boldsymbol{I} \end{bmatrix} \begin{bmatrix} \boldsymbol{I} & -\boldsymbol{C} \\ 0 & \boldsymbol{I} \end{bmatrix} = \left[\gamma_O^T, \gamma_N^T\right] \boldsymbol{B}\boldsymbol{R},$$

where γ_O denotes the hat functions in $\mathbb{V}_1$ with their apex at a node in N_0 and γ_N denotes the hat functions in $\mathbb{V}_1$ with their apex at a node in $N_1 \setminus N_0$. The matrices $\boldsymbol{C}$ and $\boldsymbol{A}$ are described above.

Once we have the relation between the two bases it is straightforward to derive a relation between the coefficients $\boldsymbol{b}$ and $(\boldsymbol{d}, \boldsymbol{w})$ of a function f_1 in the two bases.

Lemma 4. *Suppose $f_1 \in \mathbb{V}_1$ has the representation*

$$f_1 = \gamma^T \boldsymbol{b} = \boldsymbol{\phi}^T \boldsymbol{d} + \boldsymbol{\psi}^T \boldsymbol{w}$$

DOI til publisert versjon / DOI to published version: 10.1016/j.matcom.2016.09.006

in the two bases γ and $\{\phi, \psi\}$. Then the coefficients are related by

$$\begin{bmatrix} \boldsymbol{d} \\ \boldsymbol{w} \end{bmatrix} = \begin{bmatrix} \boldsymbol{I} & \boldsymbol{C} \\ 0 & \boldsymbol{I} \end{bmatrix} \begin{bmatrix} \boldsymbol{I} & 0 \\ -\boldsymbol{A} & \boldsymbol{I} \end{bmatrix} \begin{bmatrix} \boldsymbol{b}^O \\ \boldsymbol{b}^N \end{bmatrix}, \tag{20}$$

and the inverse relation

$$\begin{bmatrix} \boldsymbol{b}^O \\ \boldsymbol{b}^N \end{bmatrix} = \begin{bmatrix} \boldsymbol{I} & 0 \\ \boldsymbol{A} & \boldsymbol{I} \end{bmatrix} \begin{bmatrix} \boldsymbol{I} & -\boldsymbol{C} \\ 0 & \boldsymbol{I} \end{bmatrix} \begin{bmatrix} \boldsymbol{d} \\ \boldsymbol{w} \end{bmatrix}, \tag{21}$$

where $\boldsymbol{b}^O$ are the coefficients of the coarse hat functions γ_O with their apex at the vertices in N_0 and $\boldsymbol{b}^N$ are the coefficients of the hat functions γ_N with their apex at the new vertices $N_1 \backslash N_0$.

3.4. A local interpretation of the wavelet transforms

The two relations (20)–(21) constitute the wavelet transform and its inverse — the core algorithms for computations with wavelets. For practical implementation on triangulations, however, it is usually not advisable to form these sparse matrices. Instead, it is better to interpret (20)–(21) as operations involving a vertex and its immediate neighbours.

Equation (20) corresponds to the decomposition of f_1 into the two parts $f_0 \in \mathbb{V}_0$ and $g_0 \in \mathbb{W}_0$. It consists of two steps, namely the application of two matrices. The first step is to compute the wavelet coefficients $\boldsymbol{w} = \boldsymbol{b}^N - \boldsymbol{A}\boldsymbol{b}^O$. The vector $\boldsymbol{w}$ is conveniently indexed by the nodes $\{v_r \in N_1 \backslash N_0\}$. We consider one such node $\boldsymbol{v}_r$, which is inserted in a triangle $T_r \in \Delta_0$ formed by three nodes $\boldsymbol{v}_i, \boldsymbol{v}_j, \boldsymbol{v}_k \in N_0$. Recall that the node $\boldsymbol{v}_r$ can be expressed as the weighted sum $\boldsymbol{v}_r = a^r_j \boldsymbol{v}_i + a^r_j \boldsymbol{v}_j + a^r \boldsymbol{v}_k$, where a^r_i, a^r_j, a^r_k are the barycentric coordinates of $\boldsymbol{v}_r$. The wavelet coefficient $\boldsymbol{w}_{\boldsymbol{v}_r}$ is then given by

$$\boldsymbol{w}_{\boldsymbol{v}_r} = \boldsymbol{b}_{\boldsymbol{v}_r} - \left(a^r_i \boldsymbol{b}_{\boldsymbol{v}_i} + a^r_j \boldsymbol{b}_{\boldsymbol{v}_j} + a^r_k \boldsymbol{b}_{\boldsymbol{v}_k} \right), \tag{22}$$

the difference between the function value $\boldsymbol{b}_{\boldsymbol{v}_r} = f_1(\boldsymbol{v}_r)$ and the value at $\boldsymbol{v}_r$ of the planar function that interpolates f_1 at the vertices of T_r.

The second step in (20) is given by the relation $\boldsymbol{d} = \boldsymbol{b}^O + \boldsymbol{C}\boldsymbol{w}$. Recall that the rows of the matrix $\boldsymbol{C}$ are indexed by the nodes in N_0 (the old nodes),

DOI til publisert versjon / DOI to published version: 10.1016/j.matcom.2016.09.006

while the columns are indexed by the new nodes $N_1 \setminus N_0$. The coefficients $\boldsymbol{d}$ are conveniently indexed by the old nodes $\boldsymbol{v}_i \in N_0$, so in component form the second step becomes

$$\boldsymbol{d}_{\boldsymbol{v}_i} = \boldsymbol{b}^O_{\boldsymbol{v}_i} + (\boldsymbol{C}\boldsymbol{w})_{\boldsymbol{v}_i}.$$

The first term on the right is the contribution from the original function f_1 at the old node $\boldsymbol{v}_i$. The second part corresponds to the row of $\boldsymbol{C}$ associated with $\boldsymbol{v}_i$ multiplied with the wavelet coefficients $\boldsymbol{w}$. This row of $\boldsymbol{C}$ contains a nonzero entry c_i^r at a position $\boldsymbol{v}_r \in N_1 \setminus N_0$ if the wavelet function $\psi_{\boldsymbol{v}_r}$ is adjusted by the term $c_i^r \phi_{\boldsymbol{v}_i}$. Let L_i be the set of such indices r. We then have

$$\boldsymbol{d}_{\boldsymbol{v}_i} = \boldsymbol{b}_{\boldsymbol{v}_i} + \sum_{r \in L_i} c_i^r \boldsymbol{w}_{\boldsymbol{v}_r}. \tag{23}$$

The local relations (22) and (23) and the similar version of the inverse transform (21) provide a natural way to implement the wavelet transforms. On the other hand, the matrix form is useful for studying the stability of the wavelets, as we will see in the next section.

3.5. Analysis of stability

Let $\boldsymbol{B}$ be a nonsingular matrix. The condition number $\kappa(\boldsymbol{B}) = \|\boldsymbol{B}\|\|\boldsymbol{B}^{-1}\|$ expresses the conditioning of computing $\boldsymbol{B}\boldsymbol{x}$, i.e., how much the relative perturbation of $\boldsymbol{x}$ is magnified when $\boldsymbol{B}\boldsymbol{x}$ is computed.

In the following we will measure the stability in the $\|\cdot\|_\infty$ matrix norm induced by the ℓ^∞ vector norm $\|\boldsymbol{x}\|_{\ell^\infty} = \max_i |x_i|$. This means that the stability analysis provides bounds on the maximum perturbation error which is useful when working with geometry.

Recall that the wavelet transform is given by

$$\begin{bmatrix} \boldsymbol{d} \\ \boldsymbol{w} \end{bmatrix} = \begin{bmatrix} \boldsymbol{I} & \boldsymbol{C} \\ 0 & \boldsymbol{I} \end{bmatrix} \begin{bmatrix} \boldsymbol{I} & 0 \\ -\boldsymbol{A} & \boldsymbol{I} \end{bmatrix} \begin{bmatrix} \boldsymbol{b}^O \\ \boldsymbol{b}^N \end{bmatrix} = \boldsymbol{R}^{-1}\boldsymbol{B}^{-1} \begin{bmatrix} \boldsymbol{b}^O \\ \boldsymbol{b}^N \end{bmatrix}. \tag{24}$$

Our next task is to derive an upper bound on the condition number $\kappa(\boldsymbol{B}\boldsymbol{R})$. Since $\kappa(\boldsymbol{B}\boldsymbol{R}) \leq \kappa(\boldsymbol{B})\kappa(\boldsymbol{R})$ and both $\|\boldsymbol{B}\| = \|\boldsymbol{B}^{-1}\|$ and $\|\boldsymbol{R}\| = \|\boldsymbol{R}^{-1}\|$, we only need to derive upper bounds on $\|\boldsymbol{B}\|$ and $\|\boldsymbol{R}\|$. The norm of $\boldsymbol{B}$ and therefore $\kappa(\boldsymbol{B})$ can be determined exactly.

DOI til publisert versjon / DOI to published version: 10.1016/j.matcom.2016.09.006

Lemma 5. *The ∞-norm and condition number of the matrix $\boldsymbol{B}$ are given by $\|\boldsymbol{B}\| = 2$ and $\kappa(\boldsymbol{B}) = 4$.*

PROOF. We see from (24) that $\|\boldsymbol{B}\| = \|\boldsymbol{A}\| + 1$. Since a row of $\boldsymbol{A}$ contains the barycentric coordinates of a point in the plane, we have $\|\boldsymbol{A}\| = 1$. Then $\|\boldsymbol{B}\| = 2$ and $\kappa(\boldsymbol{B}) = \|\boldsymbol{B}\|^2 = 4$.

We now want to derive a bound on $\kappa(\boldsymbol{R})$. Note that $\|\boldsymbol{R}\| = 1 + \|\boldsymbol{C}\|$, so we only need to determine a bound on $\|\boldsymbol{C}\|$. Since the entries of $\boldsymbol{C}$ are the solutions of equations like (4), we will need to obtain an upper bound on these solutions.

Lemma 6. *The matrix $\boldsymbol{C}$ satisfies the bound $\|\boldsymbol{C}\| \leq 7/6$ and therefore $\kappa(\boldsymbol{R}) \leq (1 + 7/6)^2$.*

PROOF. We focus on a general row of $\boldsymbol{C}$ associated with an old node $\boldsymbol{v}_i \in N_0$. The nonzero entries in this row stem from triangles that have been refined and which have $\boldsymbol{v}_i$ as one of their vertices: If the entry c_i^r corresponding to the new node $\boldsymbol{v}_r$ is nonzero, this means that c_i^r is the coefficient of $\phi_{\boldsymbol{v}_i}$ in the expression (17) for $\psi_{\boldsymbol{v}_r}$. From lemma 2 we know that c_i^r satisfies a bound u_r like (13), so a bound on the norm of the row of $\boldsymbol{C}$ associated with $\boldsymbol{v}_i$ is given by the sum of all these upper bounds. Suppose further that there are a total of K refined triangles that have $\boldsymbol{v}_i$ as one of their vertices. We then need to show that

$$\frac{7}{6} - \sum_{i=0}^{K-1} u_r \geq 0. \tag{25}$$

Now let T_k for $k \in \{0, \ldots, K-1\}$ be the triangles that have $\boldsymbol{v}_i$ as a vertex, listed sequentially, in counterclockwise order, with $T_0 = T_K$ and $T_{K+1} = T_1$, as illustrated in figure 4. For $i = 0 \ldots K-1$, the area of each triangle is given by $A_i = A(T_i)$. If we insert the upper bound from lemma 2, which we note may be written as

$$\sum_{k=0}^{K-1} \frac{A_k}{\sum_{j=0}^{K-1} A_j - (A_{k-1} + A_{k+1})/7},$$

the desired inequality (25) with this notation becomes

$$\frac{7}{6} - \sum_{k=0}^{K-1} \frac{A_k}{\sum_{j=0}^{K-1} A_j - (A_{k-1} + A_{k+1})/7} \geq 0.$$

DOI til publisert versjon / DOI to published version: 10.1016/j.matcom.2016.09.006

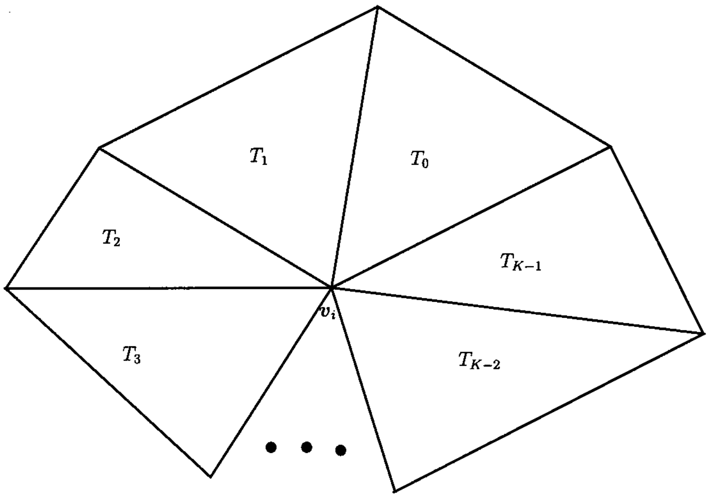

Figure 4: The triangles having v_i as one vertex.

The left-hand side of the inequality can be rewritten in a series of steps,

$$\begin{aligned}
&\frac{7}{6}\sum_{k=0}^{K-1}\frac{A_k}{\sum_{j=0}^{K-1}A_j}-\sum_{k=0}^{K-1}\frac{A_k}{\sum_{j=0}^{K-1}A_j-(A_{k-1}+A_{k+1})/7}\\
&=\sum_{k=0}^{K-1}A_k\left(\frac{7/6}{\sum_{j=0}^{K-1}A_j}-\frac{1}{\sum_{j=0}^{K-1}A_j-(A_{k-1}+A_{k+1})/7}\right)\\
&=\sum_{k=0}^{K-1}A_k\left(\frac{(7/6)\left(\sum_{j=0}^{K-1}A_j-(A_{k-1}+A_{k+1})/7\right)-\sum_{j=0}^{K-1}A_j}{\left(\sum_{j=0}^{K-1}A_j\right)\left(\sum_{j=0}^{K-1}A_j-(A_{k-1}+A_{k+1})/7\right)}\right)\\
&=\sum_{k=0}^{K-1}\frac{A_k}{6}\left(\frac{\sum_{j=0}^{K-1}A_j-(A_{k-1}+A_{k+1})}{\left(\sum_{j=0}^{K-1}A_j\right)\left(\sum_{j=0}^{K-1}A_j-(A_{k-1}+A_{k+1})/7\right)}\right).
\end{aligned}$$

The last expression is obviously nonnegative and hence the desired inequality has been established.

The coefficient 7/6 follows from the upper bound from lemma 2 with this strategy for the proof. But note that the last expression in the proof is strictly positive as long as at least one of the areas A_k is non-zero, so the bound is not sharp, and it may be possible to improve the bound.

Lemmas 5 and 6 can be summarised as an upper bound on the condition

DOI til publisert versjon / DOI to published version: 10.1016/j.matcom.2016.09.006

number of the wavelet transforms. We are also in a position to bound the coefficients of a function in $\mathbb{V}_1$ relative to one basis in terms of the coefficients in the other basis.

Theorem 7. *Let $\mathbb{V}_1$ be a space of piecewise linear functions over a triangulation T_1, refined from a space $\mathbb{V}_0$ over a coarser triangulation T_0, by strategy 1 above, and let $\mathbb{W}_0$ be the corresponding wavelet space such that $\mathbb{V}_0 \oplus \mathbb{W}_0 = \mathbb{V}_1$. The condition number $\kappa(\boldsymbol{BR})$ of the wavelet transforms between the two bases ϕ_1 and (ϕ_0, ψ_0) for $\mathbb{V}_1$ is bounded by*

$$\kappa(\boldsymbol{BR}) \leq 4(13/6)^2.$$

For a function $f \in \mathbb{V}_1$ with the two representations $\gamma^T \boldsymbol{b} = \boldsymbol{\phi}^T \boldsymbol{d} + \boldsymbol{\psi}^T \boldsymbol{w}$ in the two bases, the coefficients are bounded in terms of each other by

$$\|\boldsymbol{b}\| \leq \|\boldsymbol{d}\| + (13/6)\|\boldsymbol{w}\| \tag{26}$$

$$\|\boldsymbol{d}\| \leq (10/3)\|\boldsymbol{b}\| \tag{27}$$

$$\|\boldsymbol{w}\| \leq 2\|\boldsymbol{b}\| \tag{28}$$

PROOF. The bound for the condition number follows from lemmas 5 and 6. The inequalities for the coefficients are obtained from equations (20) and (21) by taking norms and using the triangle inequality and the matrix norms computed in this section.

Theorem 7 establishes the fact that the condition number is independent of the geometry and topology of both the initial and the refined triangulation for refinement strategy I. In the next section we verify that this is also the case for strategy II.

4. Refinement strategy II

In our second refinement strategy, we divide an edge in two, and connect opposite vertices, as shown in figure 5. The construction of the wavelets and the analysis of stability is similar to strategy I, so the description is brief.

DOI til publisert versjon / DOI to published version: 10.1016/j.matcom.2016.09.006

We now consider a node $\boldsymbol{p}$ inserted on the edge $(\boldsymbol{v}_0, \boldsymbol{v}_1)$ shared by the two triangles $T_0 = (\boldsymbol{v}_0, \boldsymbol{v}_1, \boldsymbol{v}_2)$ and $T_1 = (\boldsymbol{v}_0, \boldsymbol{v}_3, \boldsymbol{v}_1)$. The inserted node can then be expressed by the convex combination

$$\boldsymbol{p} = \lambda \boldsymbol{v}_0 + (1-\lambda)\boldsymbol{v}_1. \tag{29}$$

We construct the corresponding wavelet $\psi_{\boldsymbol{p}}$ by

$$\psi_{\boldsymbol{p}} = \gamma_{\boldsymbol{p}} - \sum_{i=0}^{3} c_i \phi_{\boldsymbol{v}_i}.$$

The coefficients are determined by requiring that $\psi_{\boldsymbol{p}}$ is orthogonal to the four coarse hat functions $\{\phi_{\boldsymbol{v}_i}\}_{i=0}^{3}$. This leads to the linear system

$$\boldsymbol{M}_{II}\boldsymbol{x}_{II} = \boldsymbol{F}_{II}, \tag{30}$$

where, by (7)–(8), the matrix $\boldsymbol{M}_{II}$ is given by

$$\boldsymbol{M}_{II} = \begin{bmatrix} \int \phi_{\boldsymbol{v}_0}\phi_{\boldsymbol{v}_0} & \int \phi_{\boldsymbol{v}_0}\phi_{\boldsymbol{v}_1} & \int \phi_{\boldsymbol{v}_0}\phi_{\boldsymbol{v}_2} & \int \phi_{\boldsymbol{v}_0}\phi_{\boldsymbol{v}_3} \\ \int \phi_{\boldsymbol{v}_1}\phi_{\boldsymbol{v}_0} & \int \phi_{\boldsymbol{v}_1}\phi_{\boldsymbol{v}_1} & \int \phi_{\boldsymbol{v}_1}\phi_{\boldsymbol{v}_2} & \int \phi_{\boldsymbol{v}_1}\phi_{\boldsymbol{v}_3} \\ \int \phi_{\boldsymbol{v}_2}\phi_{\boldsymbol{v}_0} & \int \phi_{\boldsymbol{v}_2}\phi_{\boldsymbol{v}_1} & \int \phi_{\boldsymbol{v}_2}\phi_{\boldsymbol{v}_2} & \int \phi_{\boldsymbol{v}_2}\phi_{\boldsymbol{v}_3} \\ \int \phi_{\boldsymbol{v}_3}\phi_{\boldsymbol{v}_0} & \int \phi_{\boldsymbol{v}_3}\phi_{\boldsymbol{v}_1} & \int \phi_{\boldsymbol{v}_3}\phi_{\boldsymbol{v}_2} & \int \phi_{\boldsymbol{v}_3}\phi_{\boldsymbol{v}_3} \end{bmatrix}$$

$$= \begin{bmatrix} \frac{A_0+A_1+A_3+A_4+A_7}{6} & \frac{A_0+A_1}{12} & \frac{A_0+A_3}{12} & \frac{A_1+A_4}{12} \\ \frac{A_0+A_1}{12} & \frac{A_0+A_1+A_2+A_5+A_9}{6} & \frac{A_0+A_2}{12} & \frac{A_1+A_5}{12} \\ \frac{A_0+A_3}{12} & \frac{A_0+A_2}{12} & \frac{A_0+A_2+A_3+A_6}{6} & 0 \\ \frac{A_1+A_4}{12} & \frac{A_1+A_5}{12} & 0 & \frac{A_1+A_4+A_5+A_8}{6} \end{bmatrix},$$

the right-hand side is given by

$$\begin{aligned} \boldsymbol{F}_{II} &= \begin{bmatrix} \int \phi_{\boldsymbol{v}_0}\gamma & \int \phi_{\boldsymbol{v}_1}\gamma & \int \phi_{\boldsymbol{v}_2}\gamma & \int \phi_{\boldsymbol{v}_3}\gamma \end{bmatrix}^T \\ &= \frac{1}{12}\begin{bmatrix} (\lambda+1)(A_0+A_1) & (2-\lambda)(A_0+A_1) & A_0 & A_1 \end{bmatrix}^T. \end{aligned}$$

and the vector of unknowns is

$$x_{II} = \begin{bmatrix} c_0 & c_1 & c_2 & c_3 \end{bmatrix}^T.$$

The value of λ is determined by the convex combination (29), and the explicit expressions for the integrals are found by the same procedure as in section 3.1.

DOI til publisert versjon / DOI to published version: 10.1016/j.matcom.2016.09.006

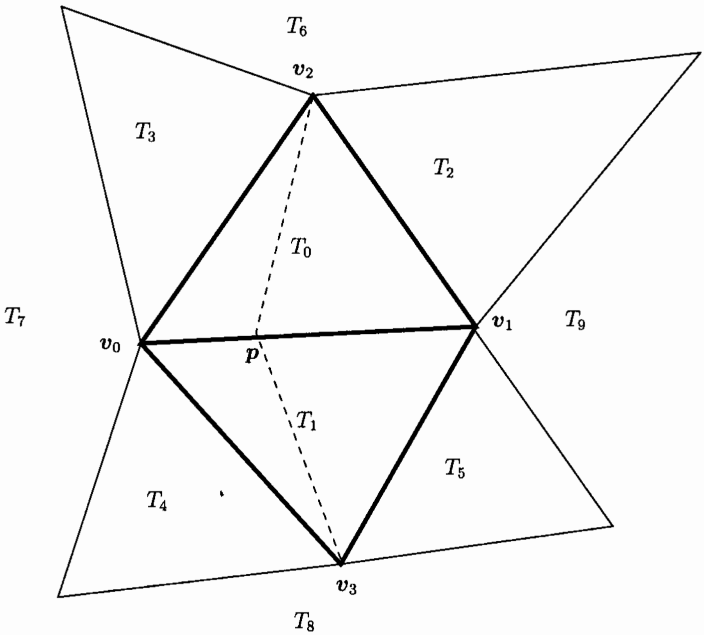

Figure 5: Overview of the areas involved in the equations for strategy 2.

DOI til publisert versjon / DOI to published version: 10.1016/j.matcom.2016.09.006

4.1. Bounds for the coefficients

As we did for the matrix $\boldsymbol{M}_I$, we partition the matrix $\boldsymbol{M}_{II}$ by its columns as $\boldsymbol{M}_{II} = [\boldsymbol{m}_1, \boldsymbol{m}_2, \boldsymbol{m}_3, \boldsymbol{m}_4]$. By Cramer's rule, the solution of (30) can be expressed by

$$\begin{aligned}
c_0 &= \frac{\det[F_{II}, \boldsymbol{m}_2, \boldsymbol{m}_3, \boldsymbol{m}_4]}{\det \boldsymbol{M}_{II}}, \\
c_1 &= \frac{\det[\boldsymbol{m}_1, F_{II}, \boldsymbol{m}_3, \boldsymbol{m}_4]}{\det \boldsymbol{M}_{II}}, \\
c_2 &= \frac{\det[\boldsymbol{m}_1, \boldsymbol{m}_2, F_{II}, \boldsymbol{m}_4]}{\det \boldsymbol{M}_{II}}, \\
c_3 &= \frac{\det[\boldsymbol{m}_1, \boldsymbol{m}_2, \boldsymbol{m}_3, F_{II}]}{\det \boldsymbol{M}_{II}}.
\end{aligned} \tag{31}$$

We want to derive a bound on these expressions and note first of all that lemma 1 also holds for $\boldsymbol{M}_{II}$, such that $D_1 > |D_i|$ for $i = 2, 3, 4$. Due to symmetry, it is sufficient to obtain a bound for one of c_0 and c_1, and one for one of c_2 and c_3. We start with c_0.

Lemma 8. *The coefficient c_0 is bounded by*

$$|c_0| \leq \frac{A_0 + A_1}{A_0 + A_1 + 2(A_3 + A_4 + A_7)/3}. \tag{32}$$

Proof. Expansion of the numerator and the denominator for c_0 show that both have only positive terms, so $c_0 \geq 0$. The expansion also shows that the maximum value for c_0 is obtained for $\lambda = 1$. The rest of the proof is similar to the proof of lemma 2.

A similar bound holds for c_1. We now turn to the coefficients c_2 and c_3.

Lemma 9. *The coefficients c_2 and c_3 are both bounded by*

$$|c_k| \leq \frac{A_0 + B_0}{\sum_{i=1}^{N} A_i + 2A_0 + 2B_0} \leq \frac{1}{2}, \quad \text{for } k = 2, 3, \tag{33}$$

where A_i for $i = 1, 2, \ldots, N$ are the areas of the triangles adjacent to $\boldsymbol{v}_k$, with $A_0 = A_N$ and $A_{N+1} = A_1$, and B_0 is the area of the neighboring triangle of A_0 which does not have $\boldsymbol{v}_k$ as a vertex, as illustrated in figure ?? for $k = 2$.

DOI til publisert versjon / DOI to published version: 10.1016/j.matcom.2016.09.006

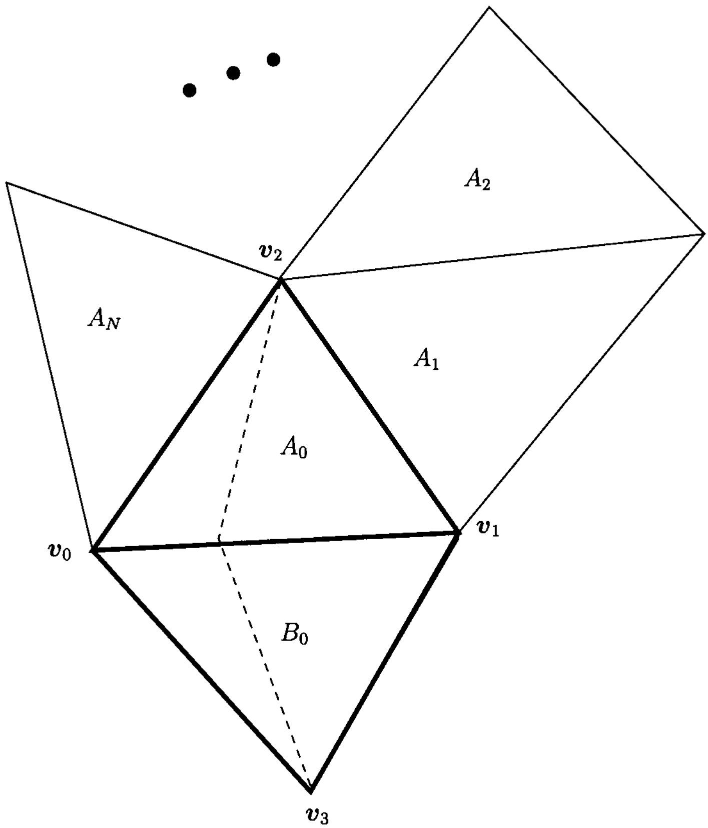

Figure 6: Overview of the areas involved in the proof of lemma 9 for $k = 2$.

DOI til publisert versjon / DOI to published version: 10.1016/j.matcom.2016.09.006

PROOF. From lemma 1, we know that the denominator is positive. Expansion of the numerator shows that it contains both positive and negative terms, and both positive and negative terms depend on the value of λ. We split the numerator into $N^+(\lambda)$ containing the positive terms and $N^-(\lambda)$ the negative terms, such that $N(\lambda) = N^+(\lambda) + N^-(\lambda)$, all being functions of λ. Then

$$\frac{N^-(1)}{\det \boldsymbol{M}_{II}} \le \frac{N^-(\lambda)}{\det \boldsymbol{M}_{II}} \le c_k \le \frac{N^+(\lambda)}{\det \boldsymbol{M}_{II}} \le \frac{N^+(1)}{\det \boldsymbol{M}_{II}},$$

since the upper and lower bounds are obtained when $\lambda = 1$ in N^+ and N^- respectively. Finally, by direct expansion one can verify that the two inequalities

$$\det \boldsymbol{M}_{II} - 2N^+(1) \ge 0, \quad \det \boldsymbol{M}_{II} + 2N^-(1) \ge 0$$

hold, and the result follows.

4.2. Analysis of stability for insertion of several nodes

The general description of the wavelet transforms in section 3.3 is also valid for strategy II. We only need to replace the matrices $\boldsymbol{A}$ and $\boldsymbol{C}$ with matrices appropriate for strategy II.

The matrix $\boldsymbol{A}$ for the second strategy is similar to the one for the first strategy. Let $\boldsymbol{v}_i$ be an old node in N_0 and let E_i denote the set of edges emanating from $\boldsymbol{v}_i$. Then the old hat function $\phi_{\boldsymbol{v}_i}$ may be expressed in terms of the new hat function $\gamma_{\boldsymbol{v}_i}$ and the new hat functions which have their apexes at the inserted nodes on the edges in E_i,

$$\phi_{\boldsymbol{v}_i} = \gamma_{\boldsymbol{v}_i} + \sum_{\boldsymbol{v}_r \in E_i} a_i^r \gamma_{\boldsymbol{v}_r}. \tag{34}$$

The vector-matrix version of this relation is

$$\boldsymbol{\phi}^T = \boldsymbol{\gamma}_O^T + \boldsymbol{\gamma}_N^T \boldsymbol{A}. \tag{35}$$

The rows of $\boldsymbol{A}$ are indexed by the new nodes in $N_1 \setminus N_0$, while the columns are indexed by the old nodes in N_0. The row associated with a new node $\boldsymbol{v}_r \in N_1 \setminus N_0$ therefore contains at most two nonzero entries, namely this node's barycentric coordinates relative to the end points of the edge where the node

DOI til publisert versjon / DOI to published version: 10.1016/j.matcom.2016.09.006

was inserted. Let E_i be the set of edges in the triangulation Δ_0 having node $\boldsymbol{v}_i$ as one end node. In the column associated with the node $\boldsymbol{v}_i$, we have one non-zero entry for each edge in E_i which has been refined with a new node.

The matrix $\boldsymbol{C}$ is based on the relation

$$\psi_{\boldsymbol{p}} = \gamma_{\boldsymbol{p}} - \sum_{i=0}^{3} c_i \phi_{\boldsymbol{v}_i} \tag{36}$$

which in matrix-vector form becomes

$$\boldsymbol{\psi}^T = \boldsymbol{\gamma}^T - \boldsymbol{\phi}^T \boldsymbol{C}.$$

Each column of $\boldsymbol{C}$ is associated with a new node $\boldsymbol{v}_r \in N_1 \setminus N_0$ and contains four non-zero entries, the coefficients c_0, c_1, c_2, c_3 for the solution of the linear system corresponding to the function $\psi_{\boldsymbol{v}_r}$. A row of $\boldsymbol{C}$ is associated with an old node $\boldsymbol{v}_i \in N_0$ and contains values of c_0, c_1, c_2 and c_3 used as a coefficient for the function $\boldsymbol{\phi}_i$ in any expression like (36). The number of nonzero entries in row i is equal to the number of refined edges emanating from the node $\boldsymbol{v}_i$. This means that a node inserted on an edge going out from $\boldsymbol{v}_i$ will only result in one entry in row i, even though it will split two of the neighboring triangles. So the number of row entries may be smaller than the number of neighboring original triangles that are split after node insertions.

As for strategy I, the matrices $\boldsymbol{B}$ and $\boldsymbol{R}$ are given by

$$\boldsymbol{B} = \begin{bmatrix} \boldsymbol{I} & 0 \\ \boldsymbol{A} & \boldsymbol{I} \end{bmatrix}, \quad \boldsymbol{R} = \begin{bmatrix} \boldsymbol{I} & -\boldsymbol{C} \\ 0 & \boldsymbol{I} \end{bmatrix}. \tag{37}$$

To bound the condition number $\kappa(\boldsymbol{BR})$ for the second strategy, we note as before that

$$\kappa(\boldsymbol{BR}) \leq \kappa(\boldsymbol{B})\kappa(\boldsymbol{R}) = \|\boldsymbol{B}\|^2 \|\boldsymbol{R}\|^2.$$

It is therefore sufficient to bound the norms of $\|\boldsymbol{B}\|$ and $\|\boldsymbol{R}\|$. By the same procedure as in lemma 5 we find that $\|\boldsymbol{B}\| = 2$ and $\kappa(\boldsymbol{B}) = 4$, since the elements of each row of $\boldsymbol{A}$ sum to 1.

The norm of $\|\boldsymbol{R}\|$ is more complicated, since we have two different bounds for the elements of $\boldsymbol{C}$. In the row associated with $\boldsymbol{v}_i$, the bound for a nonzero

DOI til publisert versjon / DOI to published version: 10.1016/j.matcom.2016.09.006

entry associated with a new node v_r is given by lemma 8 if v_r is inserted on an edge emanating from v_r, i.e., if $v_r \in E_i$. If instead the new node v_r is inserted on an edge that is not in E_i, the corresponding entry in the row is bounded by lemma 9.

We can avoid this complication if we choose our refinement strategy such that all entries in any given row of C are inserted in a similar way so that they can be bounded by the same lemma. This means that for each node $v_i \in N_0$, the new nodes inserted on the edges of triangles adjacent to v_i are either all inserted on edges in E_i, or all inserted on edges not in E_i. For now we just assume that this is possible and bound the sum of the absolute values of the entries in a row in each case.

Lemma 10. *Let v_i be a node in N_0 with valence N and emanating edges E_i, suppose that no two adjacent edges in E_i have been refined, and let c_i denote the row of C associated with v_i. Then*

$$\|c_i\|_1 \leq \frac{3}{2}$$

where $\|\cdot\|_1$ denotes the vector 1-norm.

Proof. We first assume that N is even and that every other edge around v_i has been refined. Moreover, let T_k for $k = 0, 1, \ldots, N-1$ be the triangles which have v_i as a vertex, ordered cyclically around v_i, with $T_0 = T_N$ and $T_{N+1} = T_1$, as illustrated in figure 4, and denote the area of triangle T_i by $A_i = A(T_i)$. We observe that the denominator in (32) may be rewritten as

$$A_0 + A_1 + \frac{2}{3}(A_3 + A_4 + A_7) = \frac{2}{3}(A_0 + A_1 + A_3 + A_4 + A_7) + \frac{1}{3}(A_0 + A_1).$$

Note that the first sum on the right contains the areas of all the triangles with a vertex at v_0. It is therefore sufficient to show that

$$\frac{3}{2} - \sum_{k=1}^{N/2} \frac{A_{2k-1} + A_{2k}}{\frac{2}{3}\sum_{j=1}^{N} A_j + \frac{1}{3}(A_{2k-1} + A_{2k})} \geq 0. \tag{38}$$

Since $\sum_{k=1}^{N} A_k = \sum_{k=1}^{N/2}(A_{2k-1} + A_{2k})$, the left-hand side can be written

$$\frac{3}{2}\sum_{k=1}^{N/2} \frac{A_{2k-1} + A_{2k}}{\sum_{j=1}^{N} A_j} - \sum_{k=1}^{N/2} \frac{A_{2k-1} + A_{2k}}{\frac{2}{3}\sum_{j=1}^{N} A_j + \frac{1}{3}(A_{2k-1} + A_{2k})} =$$

DOI til publisert versjon / DOI to published version: 10.1016/j.matcom.2016.09.006

$$\sum_{k=1}^{N/2}(A_{2k-1}+A_{2k})\left(\frac{\frac{3}{2}}{\sum_{j=1}^{N}A_j}-\frac{1}{\frac{2}{3}\sum_{j=1}^{N}A_j+\frac{1}{3}(A_{2k-1}+A_{2k})}\right)=$$

$$\sum_{k=1}^{N/2}(A_{2k-1}+A_{2k})\left(\frac{\frac{3}{2}\left(\frac{2}{3}\sum_{j=1}^{N}A_j+\frac{1}{3}(A_{2k-1}+A_{2k})\right)-\sum_{j=1}^{N}A_j}{\left(\frac{2}{3}\sum_{j=1}^{N}A_j+\frac{1}{3}(A_{2k-1}+A_{2k})\right)\sum_{j=1}^{N}A_j}\right)=$$

$$\sum_{k=1}^{N/2}(A_{2k-1}+A_{2k})\frac{\sum_{j=1}^{N}A_j+\frac{1}{2}(A_{2k-1}+A_{2k})-\sum_{j=1}^{N}A_j}{\left(\frac{2}{3}\sum_{j=1}^{N}A_j+\frac{1}{3}(A_{2k-1}+A_{2k})\right)\sum_{j=1}^{N}A_j}=$$

$$\frac{1}{2}\sum_{k=1}^{N/2}\frac{(A_{2k-1}+A_{2k})^2}{\left(\frac{2}{3}\sum_{j=1}^{N}A_j+\frac{1}{3}(A_{2k-1}+A_{2k})\right)\sum_{j=1}^{N}A_j}\geq 0,$$

the last inequality being obvious. If less than every other edge is refined, the outer sum in (38) contains fewer terms which means that it is easier to satisfy the inequality.

A similar argument applies if not all triangles around node $\boldsymbol{v}_i$ are split. This is the case if the valence of node $\boldsymbol{v}_i$ is odd, but may occur also for even valence if we insert new nodes on fewer than every second edge. In this case we let M denote the number of triangles that are split, and we label these triangles as T_k for $k=1,\ldots,M$, ordered cyclically around $\boldsymbol{v}_i$, such that for the kth inserted node, T_{2k-1} and T_{2k} are split. Note that since the two triangles that share a refined edge are both split, the integer M must be even. In addition, we have m triangles that are not split. These we label as T_k for $k=M+1,\ldots,M+m$, and $M+m=N$, the valence of $\boldsymbol{v}_i$. Instead of inequality (38) we now obtain from lemma 8 the following inequality that needs to be verified,

$$\frac{3}{2}-\sum_{k=1}^{M/2}\frac{A_{2k-1}+A_{2k}}{\frac{2}{3}\sum_{j=1}^{M}A_j+\frac{2}{3}\sum_{j=1}^{m}A_{M+j}+\frac{1}{3}(A_{2k-1}+A_{2k})}\geq 0. \qquad (39)$$

In order to show that this equation holds, we observe that

$$\frac{3}{2}-\sum_{k=1}^{M/2}\frac{A_{2k-1}+A_{2k}}{\frac{2}{3}\sum_{j=1}^{M}A_j+\frac{2}{3}\sum_{j=1}^{m}A_{M+j}+\frac{1}{3}(A_{2k-1}+A_{2k})}\geq$$

$$\frac{3}{2}-\sum_{k=1}^{M/2}\frac{A_{2k-1}+A_{2k}}{\frac{2}{3}\sum_{j=1}^{M}A_j+\frac{1}{3}(A_{2k-1}+A_{2k})}\geq 0,$$

where the last inequality follows from the proof of the first case.

DOI til publisert versjon / DOI to published version: 10.1016/j.matcom.2016.09.006

Lemma 11. *Let E_i be the edges emanating from the vertex $\boldsymbol{v}_0 \in N_0$, and suppose that N of the triangles which have $\boldsymbol{v}_0$ as a vertex are refined along an edge which is not in E_i. Then the entries in the row $\boldsymbol{c}_i$ of $\boldsymbol{C}$ associated with $\boldsymbol{v}_i$ is bounded by*

$$\|\boldsymbol{c}_i\|_1 \leq \frac{N}{2}.$$

PROOF. We know that there will be N nonzero entries in the row associated with $\boldsymbol{v}_i$. Lemma 9 tells us that each of these are bounded by $1/2$, and from this the result follows.

It may be possible to improve the last bound such that it becomes independent of N, but we have not been able to do so. Therefore, when strategy II is used, our bound for the norm $\|\boldsymbol{C}\|$ depends on how the strategy is applied. We will analyse our particular combination of the strategies in the next section, but end with a general result.

Theorem 12. *Let $\mathbb{V}_1$ be a space of piecewise linear functions over a triangulation T_1, refined from a space $\mathbb{V}_0$ over a coarser triangulation T_0, by strategy II, and suppose that for each node in N_0, the new nodes inserted on the edges of triangles adjacent to $\boldsymbol{v}_i$ are either all inserted on edges in E_i, or all inserted on edges not in E_i, where E_i denotes the set of edges emanating from $\boldsymbol{v}_i$. Let $\mathbb{W}_0$ be the corresponding wavelet space such that $\mathbb{V}_0 \oplus \mathbb{W}_0 = \mathbb{V}_1$. The condition number $\kappa(\boldsymbol{BR})$ of the wavelet transforms between the two bases $\boldsymbol{\phi}_1$ and $(\boldsymbol{\phi}_0, \boldsymbol{\psi}_0)$ for $\mathbb{V}_1$ is bounded by*

$$\kappa(\boldsymbol{BR}) \leq \max(25, 4 + 4K + K^2),$$

where K denotes the maximum number of triangles in Δ_0 with one common vertex. For a function $f \in \mathbb{V}_1$ with the two representations $\boldsymbol{\gamma}^T\boldsymbol{b} = \boldsymbol{\phi}^T\boldsymbol{d} + \boldsymbol{\psi}^T\boldsymbol{w}$ in the two bases, the coefficients are bounded in terms of each other by

$$\|\boldsymbol{b}\| \leq \|\boldsymbol{d}\| + (1+\alpha)\|\boldsymbol{w}\| \tag{40}$$

$$\|\boldsymbol{d}\| \leq (1+2\alpha)\|\boldsymbol{b}\| \tag{41}$$

$$\|\boldsymbol{w}\| \leq 2\|\boldsymbol{b}\| \tag{42}$$

DOI til publisert versjon / DOI to published version: 10.1016/j.matcom.2016.09.006

where $\alpha = \max(3/2, K/2)$.

PROOF. The bound for $\|C\|$ is given by the maximum of the two bounds from the lemmas 10 and 11, and the bound for the condition number follows. The inequalities for $\boldsymbol{b}$, $\boldsymbol{d}$ and $\boldsymbol{w}$ follow from equations (20) and (21).

The bounds in this section apply when either only strategy I or only strategy II is used for a one-level wavelet decomposition. For a multi-level decomposition it is possible to avoid the dependence on the topology in Theorem 12 by applying strategy II appropriately.

5. Multilevel decomposition combining strategies I and II

There are two types of approaches for construction of a hierarchy of triangulations. One is to start with a fine triangulation and remove nodes and edges to obtain the sparser triangulations in the hierarchy. Another approach is to start with a sparse triangulation and create the finer triangulations by insertion of nodes and edges. We consider the latter approach, and the flexibility of our node insertion strategies allow us to insert new nodes in areas with large errors and keep a sparse triangulation in other areas.

In this section we give a simple example of how the two node insertion techniques may be combined to construct a highly nonuniform wavelet decomposition over several levels. Once the hierarchy of triangulations has been constructed, we may determine the wavelet spaces as described above. Because of the stability results, we know that nodes may be inserted at arbitrary positions without leading to serious numerical problems.

One may construct a hierarchy of triangulations using strategy I only. This has the disadvantage that no edge will ever be split, and after some iterations the triangulations are likely to contain a number of triangles with very small angles. Although this does not adversely affect the stability of the wavelet transforms, it may be disadvantageous for other reasons. In order to avoid this, we combine strategy I with an edge dividing strategy such as strategy II. Recall

DOI til publisert versjon / DOI to published version: 10.1016/j.matcom.2016.09.006

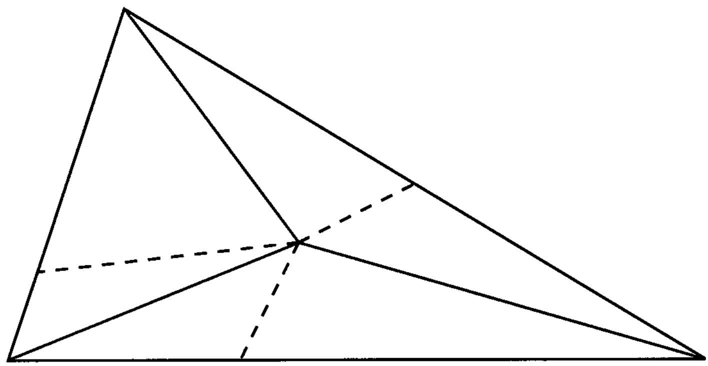

Figure 7: Combination of node insertion strategies 1 and 2.

that the condition number of the wavelet transform for strategy II has not been bounded independently of the number of node insertions around a node, see theorem 12, but it turns out that by combining strategies I and II we can avoid this dependence as we now explain.

Suppose that a new node $\boldsymbol{v}$ has been inserted in a triangle by strategy I. We then use strategy II to insert one new node on each edge of the original triangle in which $\boldsymbol{v}$ was inserted, as shown in figure 7. This means that all the original triangle edges are split into two, as is also the case for the three neighbouring triangles which share the three edges. Since $\boldsymbol{v}$ is surrounded by exactly three triangles, the bound for $\|\boldsymbol{C}\|$ in theorem 12 will become $3/2$ when strategy II is combined with strategy I in this way.

Let Δ_k be some triangulation that has been refined with strategy I, and N_k the nodes in this triangulation. We denote the set of edges in the triangulation Δ_k having node $\boldsymbol{v}_j$ as one end node by E_j. The combination of strategies I and II described above ensures that for each node $\boldsymbol{v}_i \in N_k$, the new nodes inserted on the edges of neighboring triangles are either only inserted on edges in E_i or only inserted on edges not in E_i. This means that for each row in matrix $\boldsymbol{C}$, all elements are bounded as in Lemma 10 or Lemma 11.

There will be a conflict if in strategy I we skip node insertion in only one

DOI til publisert versjon / DOI to published version: 10.1016/j.matcom.2016.09.006

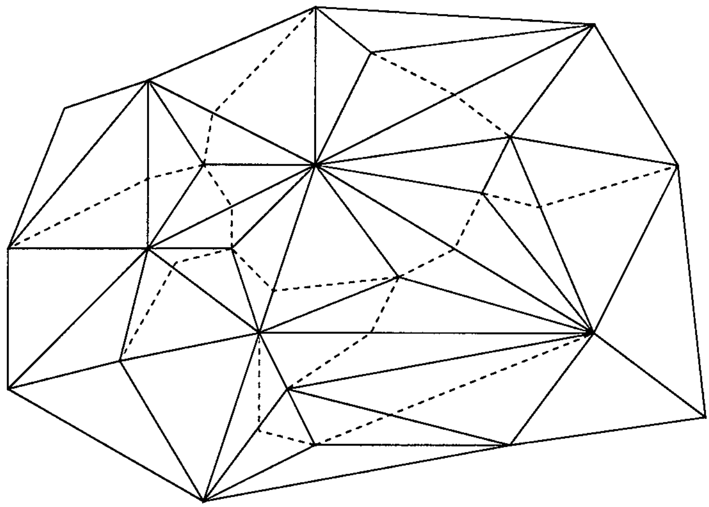

Figure 8: Combination of node insertion strategies I and II.

triangle when progressing through the triangles surrounding a node. This is because this triangle will then be divided twice in strategy II. This can be avoided for example by choosing to divide the longest edge of the empty triangle. An example of node insertion where this is done, is shown in figure 8. We see that this results in some triangles being split into four or five new triangles as opposed to the normal six new triangles after refinement by both strategies. An alternative would be to insert a new node according to strategy I in these empty triangles before continuing with strategy II.

We emphasise that the nested triangulations obtained through this strategy will normally not be considered nice triangulations, since some triangles may have very small angles and some vertices many neighbouring triangles. However these bad triangulations demonstrate well that our wavelets are stable, independently of the geometry of the triangulations.

5.1. Multilevel stability

By combining strategies I and II as indicated above, we obtain a hierarchy of triangulations, and it is then of interest to consider the stability of the wavelet

DOI til publisert versjon / DOI to published version: 10.1016/j.matcom.2016.09.006

transforms over all levels. So we consider the situation where we have a nested set of triangulations $\Delta_0 \subset \Delta_1 \subset \cdots \subset \Delta_K$, constructed alternately by strategies I and II, and corresponding nested linear spaces $\mathbb{V}_0 \subset \mathbb{V}_1 \subset \cdots \subset \mathbb{V}_K$. The final refinement from Δ_{K-1} to Δ_K is done according to strategy II, meaning that K is an even number. We can then construct wavelets in the standard wavelet tradition by applying the above recipes, such that each space $\mathbb{V}_j$ may be decomposed as $\mathbb{V}_j = \mathbb{V}_{j-1} \oplus \mathbb{W}_{j-1}$. By iterating this, the finest space $\mathbb{V}_K$ may be decomposed as

$$\mathbb{V}_K = \mathbb{V}_0 \oplus \mathbb{W}_0 \oplus \mathbb{W}_1 \oplus \cdots \oplus \mathbb{W}_{K-1}. \tag{43}$$

If we denote the basis of hat functions for $\mathbb{V}_j$ by $\boldsymbol{\phi}_j$, and the wavelet basis for $\mathbb{W}_j$ by $\boldsymbol{\psi}_j$, the decomposition (43) shows that $\mathbb{V}_K$ has the two bases $\boldsymbol{\phi}_K$ and $(\boldsymbol{\phi}_0, \boldsymbol{\psi}_0, \boldsymbol{\psi}_1, \ldots, \boldsymbol{\psi}_{K-1})$. The wavelet transforms convert a given function in $\mathbb{V}_K$ between representations in these two bases, and stability means that the condition numbers of these transforms should be bounded. This analysis is similar to the one in [9].

Since both $\boldsymbol{\phi}_K$ and $(\boldsymbol{\phi}_0, \boldsymbol{\psi}_0, \cdots, \boldsymbol{\psi}_{K-1})$ are bases for $\mathbb{V}_K$, we may represent a function f in $\mathbb{V}_K$ by

$$f = \boldsymbol{\phi}_K^T \boldsymbol{d}_K = \boldsymbol{\phi}_0^T \boldsymbol{d}_0 + \sum_{i=0}^{K-1} \boldsymbol{\psi}_i^T \boldsymbol{w}_i, \tag{44}$$

where $\boldsymbol{d}_0$ and $\boldsymbol{d}_K$ are the coefficients of the hat functions in $\boldsymbol{\phi}_0$ and $\boldsymbol{\phi}_K$ respectively, and $\boldsymbol{w}_i$ are the wavelet coefficients of the basis functions in $\mathbb{W}_i$. It is useful to collect all the coefficients on the right in (44) in a long vector

$$\boldsymbol{d} = (\boldsymbol{d}_0, \boldsymbol{w}_0, \cdots, \boldsymbol{w}_{K-1}). \tag{45}$$

The following theorem shows that the wavelet basis is stable in the L_∞-norm.

Theorem 13. *Let f be a function in $\mathbb{V}_K$ given by* (44)*, and let $\boldsymbol{d}$ denote the vector of coefficients given by* (45)*. Then*

$$\left(\frac{3}{40}\right)^{K/2} \|\boldsymbol{d}\| \leq \|f\| \leq \|\boldsymbol{d}_0\| + \sum_{i=0}^{K/2-1} \left(\frac{13}{6}\|\boldsymbol{w}_{2i}\| + \frac{5}{2}\|\boldsymbol{w}_{2i+1}\|\right).$$

DOI til publisert versjon / DOI to published version: 10.1016/j.matcom.2016.09.006

PROOF. Note first of all that $\|f\| = \|\boldsymbol{d}_K\|$. The last inequality is therefore obtained by repeated application of inequalities (27) and (41) alternately. When (27) is applied, the factor $3/10$ is gained, while when (41) is applied the factor $1/4$ is gained, i.e., a factor of $3/40$ each time both inequalities have been applied. The first inequality follows from finding the smallest lower bound for $\boldsymbol{d}_K$ by repeated use of the inequalities (27) and (41) alternately, and (28) and (42) alternately.

A standard consequence of Theorem 13 is that if the coefficients of f are perturbed, the relative error in f can be bounded by the perturbations in the coefficients. Let the perturbed function be $\hat{f} = \boldsymbol{\phi}_K^T \hat{\boldsymbol{d}}_K = \boldsymbol{\phi}_0^T \hat{\boldsymbol{d}}_0 + \sum_{i=0}^{K-1} \boldsymbol{\psi}_i^T \hat{\boldsymbol{w}}_i$. Then, if f is nonzero,

$$\frac{\|f-\hat{f}\|}{\|f\|} \leq \left(\frac{40}{3}\right)^{K/2} \frac{\|\boldsymbol{d}_0 - \hat{\boldsymbol{d}}_0\|}{\|\boldsymbol{d}\|} + \left(\frac{40}{3}\right)^{K/2} \sum_{i=0}^{K/2-1} \left(\frac{13}{6}\frac{\|\boldsymbol{w}_{2i} - \hat{\boldsymbol{w}}_{2i}\|}{\|\boldsymbol{d}\|} + \frac{5}{2}\frac{\|\boldsymbol{w}_{2i+1} - \hat{\boldsymbol{w}}_{2i+1}\|}{\|\boldsymbol{d}\|}\right), \quad (46)$$

where $\delta = (\boldsymbol{d}_0, \boldsymbol{w}_0, \ldots \boldsymbol{w}_{K-1})$.

A somewhat disappointing feature of both the estimate in Theorem 13 and the one in (46) is the presence of the factor $(40/3)^{K/2}$. This factor emerges because we repeatedly apply the estimates (26)–(28) and (40)–(42), a total of $K/2$ times.

For classical wavelets, the projection from $\mathbb{V}_k$ to $\mathbb{V}_{k-1}$ is by orthogonal projection in the L^2-norm. One advantage of this is that successive projection from $\mathbb{V}_k$ to $\mathbb{V}_{k-1}$ and then to $\mathbb{V}_{k-2}$ is equivalent to direct projection from $\mathbb{V}_k$ to $\mathbb{V}_{k-2}$. This has the consequence that when deriving multi-level stability estimates analogous to that in Theorem 13, we do not need to repeatedly apply one-level estimates, but we may estimate coefficients on level i directly in terms of coefficients on level j and thereby avoid the exponential growth.

It is worth pointing out that the estimates in Theorem 13 are not best possible. Indeed, the numerical examples below indicate that the condition numbers corresponding to the wavelets constructed here do not grow exponentially with

DOI til publisert versjon / DOI to published version: 10.1016/j.matcom.2016.09.006

the number of levels.

6. Numerical examples

We include two numerical examples to illustrate the behaviour of wavelet decomposition with the wavelets constructed here. The examples confirm that our wavelet transforms are stable, even for triangulations with small angles and vertices with a relatively large number of neighbouring triangles, i.e. high *valence*. For most purposes, such triangulations are viewed as bad and are tried to be avoided.

We use a dataset of a mug that was obtained using a laser scanner. This dataset consists of points in the xy-plane, with a depth value z at each point. Based on the dataset, we create a sparse initial triangulation. Through refinements with strategies I and II alternately, as described in section 5, we establish a hierarchy of nested triangulations. We start with strategy I and end with strategy II. We have applied the strategies such that they only refine the interior of the triangles and edges, so the boundary of the initial triangulation will remain unchanged.

When refining a triangle with strategy I, we have chosen to insert the new node at the position corresponding to the data point that has the z-value that deviates the most from the plane interpolating the dataset at the vertices of the triangle. In the first example we have added the restriction that the barycentric coordinates of the new point should be greater than 0.3. This is to avoid triangles with extremely small angles. In the second example we accept any nonnegative values of the barycentric coordinates for the new point.

In strategy II a given triangulation is refined by inserting new nodes on edges. However, only in rare cases will the original dataset contain points that lie exactly on an existing edge. To circumvent this problem, we augment our dataset with new, artificial data points. We have chosen to insert the new nodes such that the two new edges that connect the two vertices opposite the edge, form a straight line. However, in some cases the straight line between these

DOI til publisert versjon / DOI to published version: 10.1016/j.matcom.2016.09.006

Level	$\|C\|_\infty$	
	Strategy 1	Strategy 2
0	0.592904	
1		0.652707
2	0.562035	
3		0.723849

Table 1: The norm of matrix C for barycentric coordinates greater than 0.3.

two vertices will intersect the edge close to, or beyond, an end point. In such situations we insert a node, somewhat arbitrarily, at a relative distance of 10 % from the end node that is closest to the intersection. The corresponding z-value is determined from the plane interpolating the three nearest points in the dataset.

After the desired number K of refinements is reached, we use the piecewise linear interpolant $f_K \in \mathbb{V}_K$ over the finest triangulation as the starting point for the wavelet decompositions. In the two examples reported here, we have used $K = 4$. We then compute the wavelet coefficients successively. The results are shown in figures 9 and 10 and tables 1 and 2, respectively. As expected, all computed functions behave nicely.

We emphasise that this construction of nested triangulations is merely a tool for demonstrating the robustness of our wavelet construction — for most practical applications more sophisticated constructions would be necessary.

7. Conclusion

We have shown how to construct piecewise linear, wavelet-like functions over a hierarchy of triangulations. The hierarchy is constructed by refinement according to one of two refinement strategies described in this paper, or a combination of these. The first refinement strategy inserts at most one new node in the interior of each triangle, while the second strategy divides edges into two

DOI til publisert versjon / DOI to published version: 10.1016/j.matcom.2016.09.006

Level	$\|C\|_\infty$	
	Strategy 1	Strategy 2
0	0.698621	
1		0.758566
2	0.832565	
3		0.842255

Table 2: The norm of matrix C for barycentric coordinates greater than 0.

pieces. We have analyzed the stability of the wavelet-like functions for each of these refinement strategies. For the first strategy, the construction is shown to be stable independently of the topology and the geometry of the initial triangulation and the refinement. For the second strategy, we have shown that the construction is stable independently of the geometry of the initial triangulation and the refinement, but our estimates do depend on the topology.

We have also analyzed a refinement strategy, which combines the two basic strategies in such a way that the stability estimates become completely independent of the triangulations. We have included two examples which demonstrate the performance of this refinement strategy.

This work has some obvious generalizations and extensions. There are many other ways to refine triangles than the ones we have considered here, all of which would require a stability analysis. There are also possible improvements of the work in this paper. The most obvious improvement is to remove the dependence on N, i.e., the triangulation, in Lemma 11. A seemingly more challenging problem is to confirm the behaviour in the numerical examples and estimate directly the conditioning of projection form a space $\mathbb{V}_i$ to an arbitrary coarser space $\mathbb{V}_j$, without going via the intermediate spaces.

References

[1] C. Chui, An Introduction to Wavelets, Academic Press, Boston, 1992.

DOI til publisert versjon / DOI to published version: 10.1016/j.matcom.2016.09.006

[2] A. Cohen, I. Daubechies, J.-C. Feauveau, Biorthogonal bases of compactly supported wavelets, Comm. on Pure and Appl. Math. 45 (5) (1992) 485–560.

[3] W. Dahmen, A. Kunoth, K. Urban, Biorthogonal spline wavelets on the interval—stability and moment conditions, Appl. Comput. Harmonic Anal. 3 (1999) 132–196.

[4] I. Daubechies, Ten Lectures on Wavelets, Soc. for Ind. and Appl. Math., 1992.

[5] I. Daubechies, I. Guskov, P. Schröder, W. Sweldens, Wavelets on irregular point sets, Phil. Trans. R. Soc. Lond. A 357 (1999) 2397 2413.

[6] M. Floater, E. Quak, Linear independence and stability of piecewise linear prewavelets on arbitrary triangulations, Soc. for Ind and Appl. Math. J. on Numer. Anal. 38 (1) (2000) 58–79.

[7] D. Hardin, D. Hong, Construction of wavelets and prewavelets over triangulations, J. of Comput. and Appl. Math. 155 (2003) 91–109.

[8] T. Lyche, K. Mørken, E. Quak, Theory and algorithms for non-uniform spline wavelets, Multivar. Approx. and Appl. (2001) 152–187.

[9] T. Lyche, K. Mørken, F. Pelosi, Stable, linear spline wavelets on nonuniform knots with vanishing moments, Comput. Aided Geom. Des. 26 (2) (2010) 203–216.

[10] R. Stevenson, Stable three-point wavelet bases on general meshes, Numerische Mathematik 80 (1998) 131–158.

[11] R. Stevenson, Locally supported, piecewise polynomial biorthogonal wavelets on nonuniform meshes, Constr. Approx. 19 (2003) 477–508.

[12] W. Sweldens, P. Schröder, Building your own wavelets at home, in: Wavelets in Computer Graphics, ACM SIGGRAPH Course notes, 1996, pp. 15–87.

DOI til publisert versjon / DOI to published version: 10.1016/j.matcom.2016.09.006

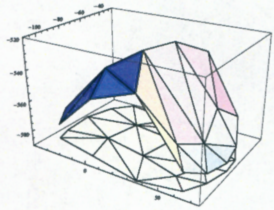

(a) mugV0

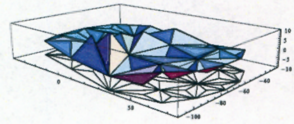

(b) mugW0

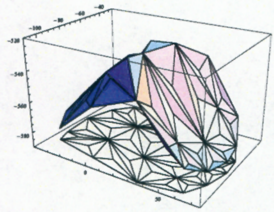

(c) mugV1

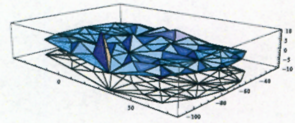

(d) mugW1

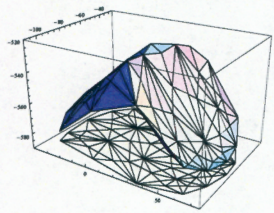

(e) mugV2

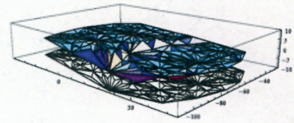

(f) mugW2

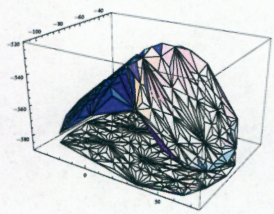

(g) mugV3

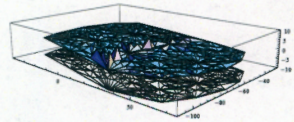

(h) mugW3

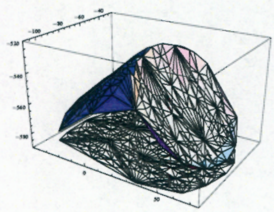

(i) mugV4

Figure 9: Wavelet decomposition of a mug. Here we require the barycentric coordinates to be greater than 0.3 in strategy 1.

DOI til publisert versjon / DOI to published version: 10.1016/j.matcom.2016.09.006

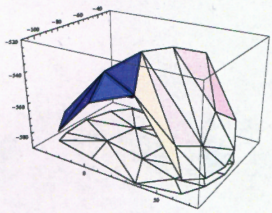

(a) mugV0

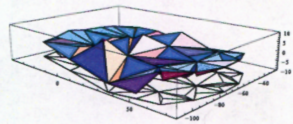

(b) mugW0

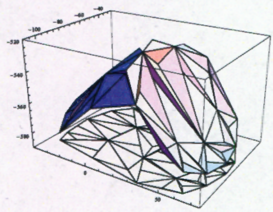

(c) mugV1

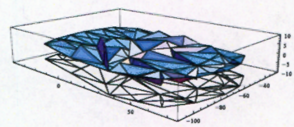

(d) mugW1

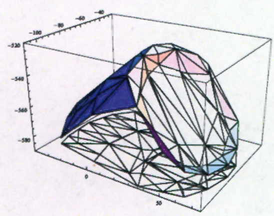

(e) mugV2

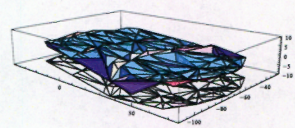

(f) mugW2

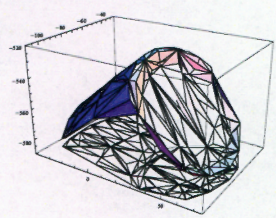

(g) mugV3

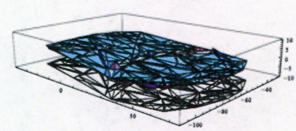

(h) mugW3

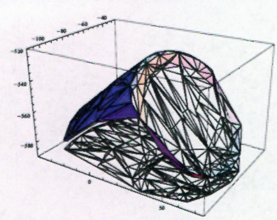

(i) mugV4

Figure 10: Wavelet decomposition of a mug on a triangulation, allowing any barycentric coordinates in strategy 1.

DOI til publisert versjon / DOI to published version: 10.1016/j.matcom.2016.09.006